ORCA – Online Research @ Cardiff

Identification of single site gold catalysis in acetylene hydrochlorination

Grazia Malta[a], Simon A. Kondrat[a], Simon J. Freakley[a], Catherine J. Davies[a], Li Lu[b], Simon Dawson[a], Adam Thetford[c,d] Emma K. Gibson[c,d], David J. Morgan[a], Wilm Jones[c], Peter P. Wells[c,d,e], Peter Johnston[f], C. Richard A. Catlow[a,c,d] Christopher J. Kiely[b] and Graham J. Hutchings[a*]

[a] Cardiff Catalysis Institute, School of Chemistry, Cardiff University, Main Building, Park Place, Cardiff, CF10 3AT, UK.

[b] Department of Materials Science and Engineering, Lehigh University, 5 East Packer Avenue, Bethlehem, Pennsylvania, PA 18015, USA.

[c] UK Catalysis Hub, Research Complex at Harwell, RAL, Oxford, OX11 0FA, UK.

[d] Kathleen Lonsdale Building, Department of Chemistry, University College London, Gordon Street, London, WC1H 0AJ, UK.

[e] School of Chemistry, University of Southampton, Southampton, SO17 1BJ, UK.

[f] Process Technologies, Johnson Matthey PLC, Billingham TS23 1LB, UK.

* hutch@cf.ac.uk

Abstract

There remains considerable debate over the active form of gold under operating conditions of a recently validated gold catalyst for acetylene hydrochlorination, . We have performed an in situ x-ray absorption fine structure study of Au/C catalysts under acetylene hydrochlorination conditions and show that highly active catalysts comprise single-site cationic Au entities whose activity correlates with the ratio of Au(I) : Au(III) present. We demonstrate that these Au/C catalysts are supported analogs of single-site homogenous Au catalysts and propose a mechanism, supported by computational modelling, based on a redox couple of Au(I) : Au(III) species.

A major environmental landmark occurred in late 2015 with the commercialization of carbon-supported gold as a catalyst for acetylene hydrochlorination in China (*1, 2*). Since the 1950s, mercuric chloride supported on carbon has been used as a catalyst for the production of vinyl chloride monomer (VCM) via this reaction. In 1985, Hutchings predicted (*3*) that gold should be the best catalyst for this reaction and subsequently showed this to be the case by experiment (*4*). During the past decade, the manufacture of VCM has increased markedly in China, partly because of the availability of coal as a feedstock for acetylene production. However, this trend has increased the environmental burden resulting from mercury pollution and, with the signing of the Mimimata accord (*5*), a replacement for mercuric chloride in the acetylene hydrochlorination reaction was mandated. The use of carbon-supported gold for this reaction represents the first time in more than 50 years that there has been a total change in the catalyst composition for the manufacture of a major commodity chemical.

The key question that remains is 'What is the nature of the active gold species under acetylene hydrochlorination reaction conditions*?*' Ex-situ spectroscopy and electron microscopy (*6-9*) studies have suggested that gold nanoparticles are present and the active sites are cationic gold associated with these nanoparticles (*6, 10*). Recently, a possible role for Au(I) as well as Au(III) has been implicated in acetylene hydrochlorination (*11*) and other reactions (*12, 13*). Since the original disclosure of gold as an effective catalyst for alkyne transformations (*14*), numerous

examples of Au(I) complexes have been described for such reactions, which suggests that the active gold catalyst for acetylene hydrochlorination could be a supported gold cation. Single gold cations have been implicated in heterogeneous catalysts before (*15-17*), but these materials either deactivate rapidly or form substantial concentrations of gold clusters or nanoparticles after reaction. We have now performed in situ x-ray absorption fine structure (XAFS) experiments to definitively show that the active catalyst for acetylene hydrochlorination predominantly comprises of Au(I) isolated cationic species analogous with the single-site homogeneous catalysis afforded by Au(I) complexes (*19,20*). For an in situ XAFS study of these homogeneous gold catalysed reactions, see (*21*).

A series of 1 wt% Au materials supported on carbon powder were prepared by impregnation with $HAuCl_4$ dissolved in either aqua regia, HNO_3, or H_2O by previously described methods (designated as Au/C-AR, Au/C-HNO_3 and Au/C-H_2O respectively) (*11*). Scanning transmission electron microscopy (STEM) analysis of the Au/C-AR catalyst (Fig. 1A) revealed the presence of predominantly highly dispersed isolated Au species. Some dimeric Au species were also identified, although they were a relatively minor component compared to the isolated monomeric Au species (Figure S1) (*22*). This finding was supported by x-ray diffraction (XRD) (Fig. 1B), where no reflections associated with metallic Au nanoparticles were observed. The lack of long-range order was further corroborated by extended x-ray absorption fine structure (EXAFS) analysis (Fig. 1C), where no Au-Au characteristic distances were detected. In addition, substantial contributions from Au-Cl entities can be seen in the EXAFS Fourier transform (FT). Fitting a first coordination shell for Au-Cl gave an average coordination number (CN) of 2.6 [Table S1] (*22*). Furthermore, ex-situ Cl K-edge XANES studies confirmed the presence of Au-Cl bonding (Figure S2) (*22*).

Further information on Au speciation can be determined from the normalized Au L_3 edge x-ray absorption near edge structure (XANES) (see experimental SM section for full details) (*22*). The white-line intensity (a strong adsorption feature associated with Au $2p_{3/2}$ core electron excitation to unoccupied 5d or 6s states) is indicative of 5d-band occupancy; Au species with higher oxidation states (*i.e.* reduced 5d electron occupancy) have stronger white-line adsorption features. Analysis of the white-line intensity during XANES measurements, when compared to appropriate standards, has precedence in the literature as a reliable method of identifying Au oxidation state (*23, 24*). The typical normalized white-line intensity values observed for cationic Au standards of Au(III) (*e.g.,* $KAuCl_4/[AuCl_4]^-$) and Au(I) (*e.g.* $[AuCl_2]^-$) are 1.1 and 0.6 respectively and correlate well with measured values from our chosen standard materials

(Figure S3) (*22, 23, 25*). The white-line intensity (Fig. 1D) of the fresh Au/C-AR catalyst was 0.78, indicating a substantially oxidized Au speciation, with linear combination fitting showing no contribution from Au^0 (within fitting error), 56% from $[AuCl_2]^-$ and 44% from $[AuCl_4]^-$ (Table S2) (*22*). Notably, we have not relied upon x-ray photoelectron spectroscopy (XPS) for characterization because of observable beam-induced photoreaction of Au^{3+} salts (Figure S4) (*22*), which will overstate Au^0 content in the Au/C catalysts. Photoreduction did not occur with synchrotron radiation in the XAFS technique because of the higher photon incident energy, which results in a significantly lower absorption cross section compared with XPS (Figure S4) (*22*).

The Au/C-AR catalyst has an induction period typically of 1 hour , strongly suggesting that its active form is generated under reaction conditions (*11*). To investigate the nature of the Au species under in situ acetylene hydrochlorination reaction conditions, we used a purpose-built micro-reactor to perform XAFS analysis while following the reaction by mass spectrometry (see experimental for details) (*22*). Under the dilute reaction conditions (2.36% C_2H_2 and 2.40% HCl) that we needed with this apparatus, we observed increasing acetylene conversion with increasing time-on-line . However, the induction period occurred over a longer timespan (3 h) under these dilute conditions (Fig. 2A). All of the Au/C catalysts we tested were highly selective toward VCM; no dichloroethene or chloroethane products were detected at any level of acetylene conversion.

We used in situ XAFS to monitor changes in Au speciation of the Au/C-AR catalyst upon heating to reaction temperature (200°C) under an inert atmosphere prior to the addition of reactants. On heating, a decrease in white-line intensity from 0.78 at 25°C to 0.68 was observed, which suggests a change from a mixed Au(III)/Au(I) chloride speciation to a Au(I) chloride-like species. This change correlates well with the decomposition temperature of $AuCl_3$ to AuCl that occurs at ~160 °C. (*26*) The white-line intensity was stable at 0.68 during the 30 min isotherm at 200 °C prior to the addition of reactant gases (Figure S5) (*22*). The continued absence of any detectable Au-Au distances in the catalyst indicates that the Au remained in a highly dispersed state.

Further analysis of the Au/C-AR catalyst showed that upon introduction of the reactant gases, an immediate change in the Au L_3 edge XANES spectrum occurred (Fig. 2, A and B). The white-line intensity increased from 0.68 to 0.94 during the first 20 min time-on-line, and then steadily decreased back to a stable value of 0.72 after ~180 min. This observation suggests that

Au(I) chloride-type species initially present were oxidized to predominantly Au(III) chloride species by the reactants during the first 20 min, and during the subsequent 160 min of reaction, the average oxidation state of the Au species gradually moved back toward that of Au(I) before converging to a stable condition somewhere between the two extremes. After the initial 15 min time on line, where reaction conditions reached steady-state, the measured change in relative white-line intensity correlated strongly with the simultaneously recorded VCM productivity of the catalyst (Pearson's r value of -0.995 as shown in Figure S6) (*22*) , with higher productivity being observed with lower Au white-line relative intensity. Importantly; no characteristic Au-Au distances were measurable by EXAFS while the catalyst was producing VCM during the entire reaction period (Figure S7a) (*22*). Linear combination fitting analysis of XANES spectral data with $[AuCl_4]^-$, $[AuCl_2]^-$ and Au-foil standard spectra showed a trend similar to that deduced from the white line intensity analysis (Figure S8a) (*22*). However, poor R fitting values in the linear combination fitting (Figure S9) (*22*) implies that our interpretation of the XANES spectral changes being solely associated with variations in the relative concentrations of $[AuCl_4]^-$ and $[AuCl_2]^-$ could be an oversimplification. XANES spectra are influenced by the hybridization of substrate molecule and metal d band orbitals (*27, 28*) and by changes in metal speciation geometry through interaction with the support (*29*). Both these reported complications are conceivable in this work, in the form of (i) interactions between the acetylene π- and Au (5d) orbitals and (ii) $C\text{-}AuCl_x$ geometric effects. However, we observed a linear correlation between white-line intensity and the EXAFS derived Au-Cl co-ordination number (CN), at a range of reaction times (Figure S10) (*22*), which supports our interpretation of the white-line intensity as being directly associated with changes in the Au-Cl speciation. Analysis of the spent catalyst by STEM-HAADF imaging confirmed the prevalence of atomically dispersed Au species as well as some occasional sub-nm clusters, but there was a total absence of any metallic Au nanoparticles (Fig. 2C).

To further re-enforce our findings, we performed comparable in situ XAFS studies, along with reaction effluent analysis, on corresponding Au/C catalysts prepared with nitric acid or water. The Au/C-HNO₃ catalysts were reported to have some activity and display comparable induction periods to the Au/C-AR catalyst (*11*) which was also extended by the dilute reaction conditions. Ex-situ characterization of the Au/C-HNO₃ sample showed lower Au dispersion when compared to Au/C-AR, with some evidence of metallic Au particles from XRD (Figure S11) (*22*). However, in situ EXAFS and XANES of Au/C-HNO₃ under reaction conditions showed that the active stable catalyst was still predominantly comprised of cationic $AuCl_x$

species (Figures S7b and S8b) (*22*). The same correlation between Au L$_3$ edge white-line intensity and catalytic activity as found for Au/C-AR materials was observed (Fig. 3A). However, the catalytic activity of the Au/C-H$_2$O material, when measured under more concentrated reaction mixtures (*11*), was very low and showed no improvement with reaction time-on-line. This catalyst was comprised predominantly of metallic Au nanoparticles (as observed from XRD, Figure S11, and STEM, Figure S12) (*22*), and no white-line was observed in XANES (Fig. 3A) indicating very low concentrations of dispersed Au species. Indeed, this catalyst was the only one we investigated that had discernible Au-Au scattering paths in the FT of the EXAFS data and showed no characteristic Au-Cl distances (Fig. 3B). Under reaction conditions, almost no change was observed in the in situ XANES or EXAFS spectra (Figures S7c and S8c) (*22*).

We also prepared a Au/C catalyst using Au(I)-thiosulfate as a precursor complex (designated Au/C-S$_2$O$_3$) that was more stable and active catalyst under reaction conditions than those made with the Au-Cl precursor. We have demonstrated that use of a more stable cationic gold complex prepared from a range of sulphur containing ligands, such as thiosulfate, results in highly active catalysts at low gold loadings (*1, 30*)(*1*). The catalytic activity of Au/C-S$_2$O$_3$ was similar that of the steady state activity of the Au/C-AR and Au/C-HNO$_3$ catalysts (Fig. 3A), but it had no induction period. As with the Au/C-AR and Au/C-HNO$_3$ materials, EXAFS analysis of the fresh Au/C-S$_2$O$_3$ sample showed no Au-Au distances and a substantial contribution from a Au scattering path with a low atomic number neighbour (Fig. 3B). Given the similar nature of Cl and S from an EXAFS perspective and Au-thiosulphate complexes having two Au-S bonds with an angle near 180° (*31*) (almost identical to the molecular geometry of [AuCl$_2$]$^-$), we cannot distinguish between Au-Cl and Au-S scattering paths by EXAFS. A fitting of the EXAFS data from the fresh Au/C-S$_2$O$_3$ catalysts (Table S1) (*22*) gave a CN of 2.0 (±0.1), showing that the Au-bonded species was the Au-thiosulfate complex. This CN corresponded well with the white-line intensity of 0.68, further showing that the catalyst comprised predominantly Au(I) species before reaction (Fig. 3A). Interestingly, upon the addition of the reactant gases, a slight increase in white-line intensity to 0.78 (with concomitant Au-S and/or Au-Cl CN of 2.6) was observed after 30 min, indicating oxidation of some of the Au-species to Au^{3+} (Fig. 3A). This increase in CN above the initial value of 2.0 shows that Cl is coordinated to the Au-thiosulphate complex. Importantly, the increase in white-line intensity was far less than that with the Au/C-AR catalyst, which is consistent with the lack of induction period for the Au/C-S$_2$O$_3$ catalysts. As with Au/C-AR materials, both EXAFS and STEM-

HAADF imaging studies (Figures S7d and S13) (22) of the Au/C-S$_2$O$_3$ catalysts showed that the Au was almost entirely in an atomically dispersed form (with only a few dimeric species) on the C support both before and after the in situ experiments. We note that the relative white-line intensity of the Au/C-S$_2$O$_3$ catalyst at steady state was the same as for the Au/C-AR catalyst at similar activity.

Figure 3C shows that a correlation can be made between the white-line intensity and VCM production of the three active catalysts (Au/C-AR, Au/C-HNO$_3$ and Au/C-S$_2$O$_3$) throughout their induction periods and at steady state. Across all three catalyst sample sets, which we have shown to be cationic in nature, the VCM productivity can be correlated with white-line adsorptions suggesting the highly dispersed Au(I) species are crucially important for this reaction and that similar oxidation state species are responsible for the activity in these catalyst systems. However, in all catalysts that are highly active, there is also a population of highly dispersed Au(III) like species present which could suggest, as originally predicted using correlations with standard electrode potential (3), that the activity is related to a Au(I) – Au(III) redox couple. Mechanistically, the reaction could be hypothesised to proceed through the oxidative addition of HCl to Au chloride, followed by the addition of acetylene and reductive elimination of VCM through a Au(I) – Au(III) redox couple. This mechanism has generally been disregarded, as it requires Au$^+$ as opposed to the more frequently observed Au(III)(32). However, under steady state conditions, the Au(I)/Au(III) ratio is ~ 1.5, and that activity can be correlated to the presence of Au(I), as observed in several homogeneous systems ($33,34$).To investigate the role of Au(I) further, we have also undertaken a Density Functional Theory (DFT) study of the interaction of HCl with supported Au species (Fig. 4). Here we focus on Au(I), by investigating AuCl on a graphite surface cut in the (119) index plane and hydroxylated on the step edge to stabilise the edge, which is described in detail in the supplementary information. HCl is added across the AuCl to form AuCl$_2$H with a barrier of 98 kJ mol^{-1}. This species shows a higher Hirshfeld charge of 0.37e compared to 0.19e for the AuCl. The former value is similar to Au(III) which has a charge of 0.41e, when modelled as AuCl$_3$, indicating that this species has more Au(III) character. The most stable configuration for a HCl molecule interacting with AuCl has a binding energy of -131 kJ mol^{-1}, which compares with -73 kJ mol^{-1} for AuCl$_2$H. Dissociation of the HCl is inhibited by hydrogen-bonding interactions; moreover, this site can be easily blocked by additional HCl and other paths for dissociation are less favorable as HCl has a lower adsorption energy of -52 kJ mol^{-1}. The generation of VCM can occur via AuCl$_2$(C$_2$H$_3$), which has an increased stability compared

to $AuCl_2H(C_2H_2)$ with a binding energy of -224 kJ mol^{-1} compared to -128 kJ mol^{-1}. VCM is further stabilized with a binding energy of -269 kJ mol^{-1} but this can be displaced by HCl. The theoretical mechanism, combined with the observation that under in situ conditions the active site is a support gold cation, with a catalytic cycle involving Au(I) and Au(III), confirms the original prediction concerning gold being the best catalyst for this reaction based on its standard electrode potential (*3*).

Fig. 1. Characterization of a freshly prepared 1 wt % Au /C-AR catalyst. (**A**) Representative HAADF-STEM image showing isolated Au species. (**B**) Powder x-ray diffraction data of this catalyst. (**C**) Fourier transform of k^3 weighted χ EXAFS ex-situ data of the sample and a gold foil reference. Variation in magnitude of Fourier transform is plotted with distance R from the Au absorber. (**D**) Ex-situ Au L$_3$-edge normalised XANES spectra of the sample and a gold foil reference material.
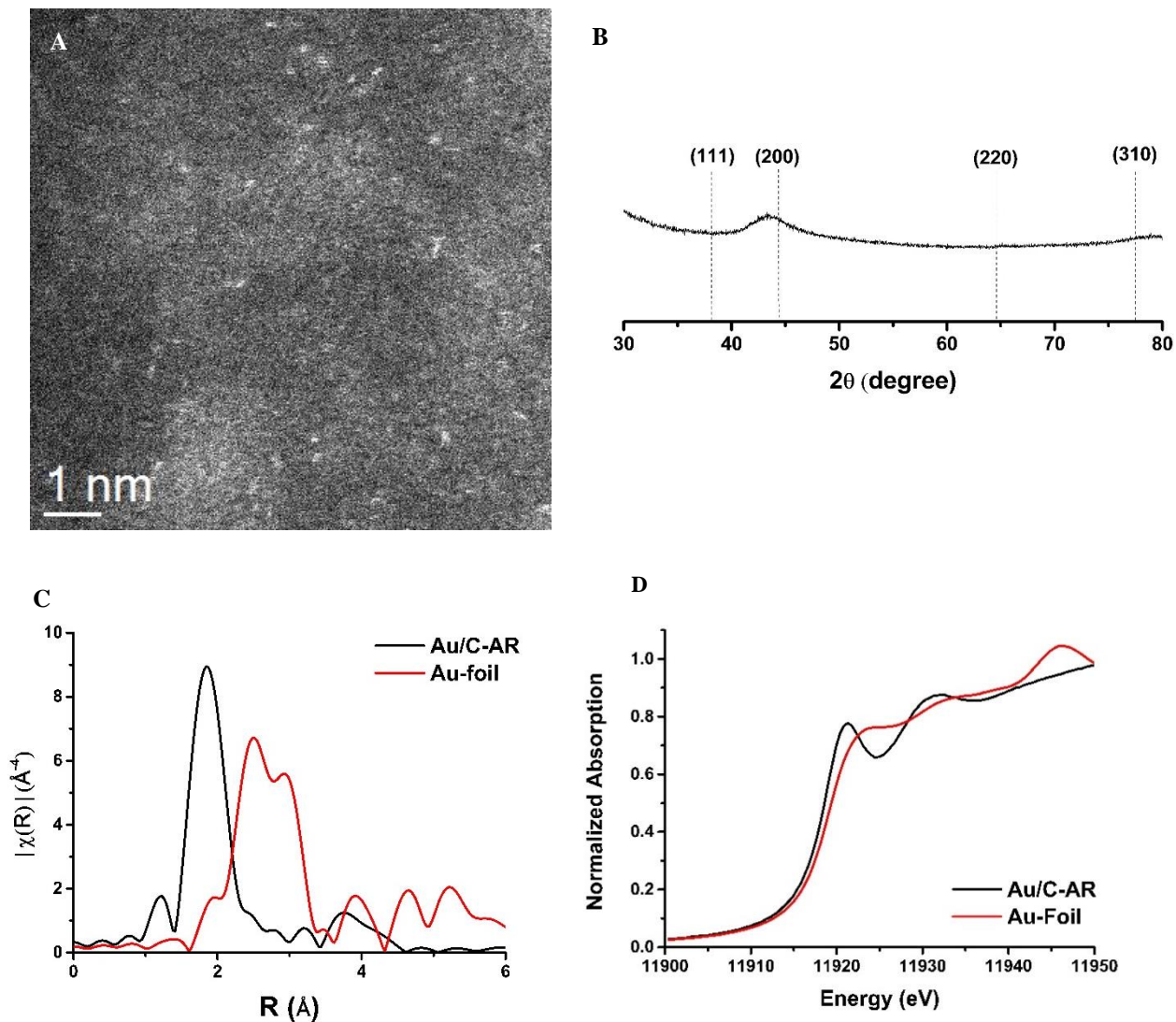
Fig. 2. VCM productivity and in situ characterization of 1 wt % Au/C-AR catalyst as a function of time-on-line. (**A**) Catalytic performance as a function of time-on-line (black) and the change in normalised white line intensity (blue) as function of reaction time. (**B**) 3D profile plot of successive Au L_3-edges from XANES spectra acquired in situ as a function of reaction time. (**C**) Representative HAADF-STEM image of Au/C-AR after use for 240 min showing the presence of atomically dispersed species and a few occasional sub-nm clusters.
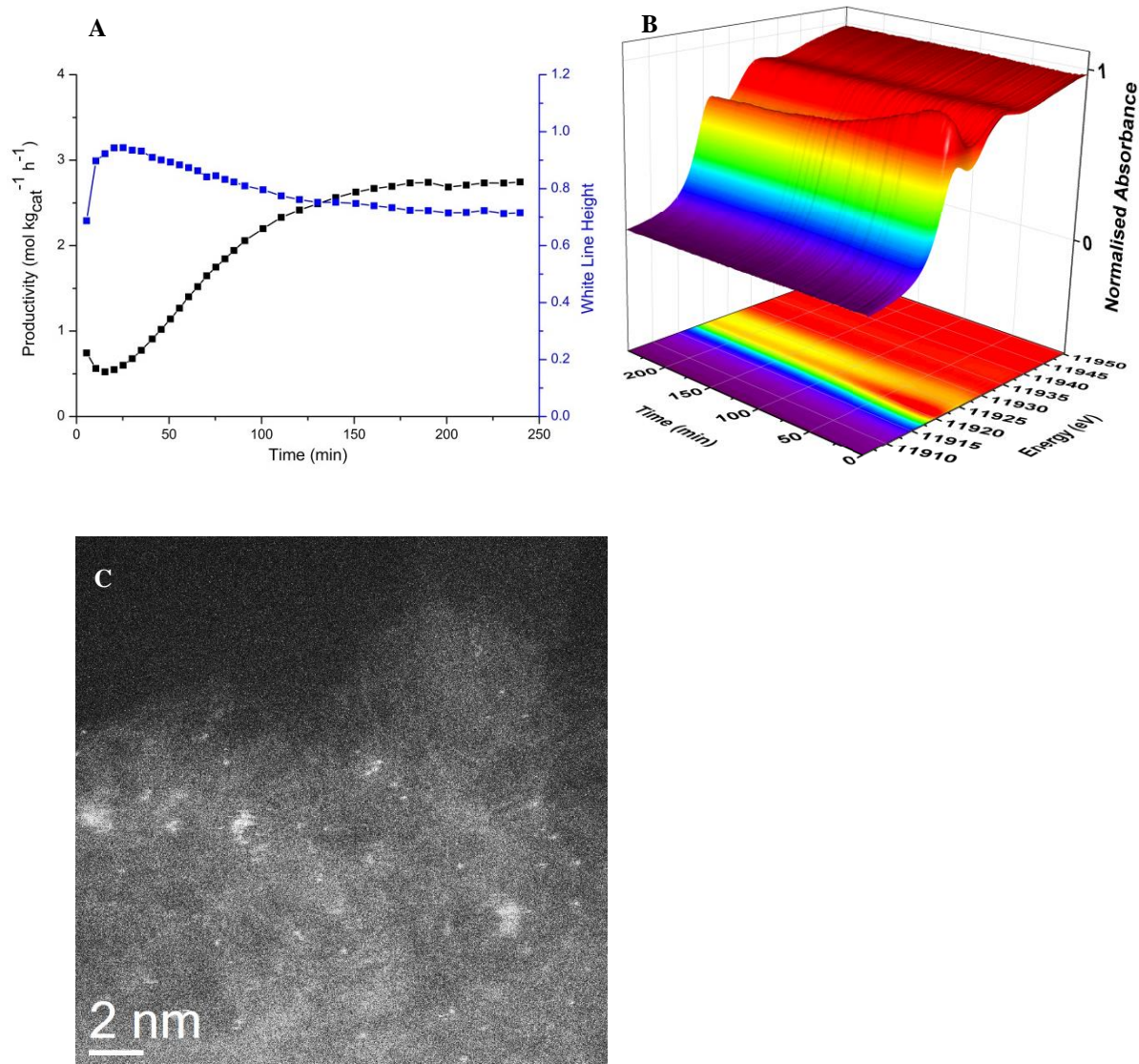
Fig. 3. VCM productivity and in situ XAFS characterization of alternatively prepared 1 wt % Au/C catalysts (**A**)Catalytic activity (black line) as a function of time-on-line for the catalysts prepared with nitric acid, thiosulphate, and with water; the blue lines show the corresponding change in relative white line intensity as function of reaction time. (**B**) k^3 weighted EXAFS Fourier Transform data for (black) 1 wt % Au/C-HNO$_3$, (blue) 1 wt % Au/C-S$_2$O$_3$ and (green) 1 wt % Au/C-H$_2$O and reference gold foil (red). (**C**) Dashed lines represent the white line intensities of the Au(I) [AuCl$_2$]$^-$ standard (value of 0.6) and the Au(III) KAuCl$_4$ standard (value of 1.1). [AuCl$_2$]$^-$ standard from difference spectra calculated in (18).
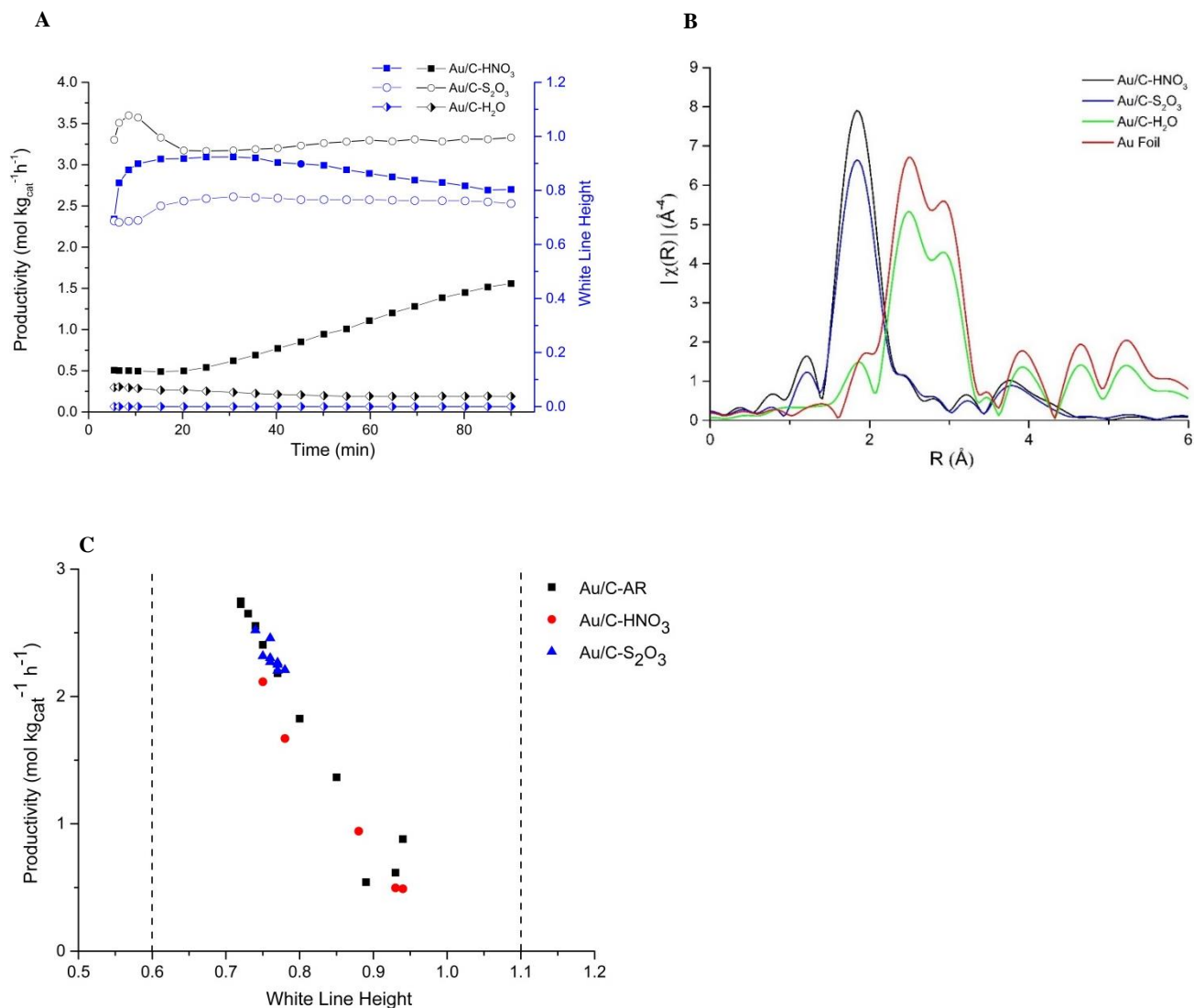
Fig. 4. Mechanism for the transformation of AuCl to AuCl₂H and formation of VCM reproducing AuCl. Key:- Au atoms (gold), Cl atoms (green), H atoms (white), C atoms (grey) and O atoms (red). Energies are given with reference to the geometry optimized configuration of AuCl on the carbon support and gas phase acetylene and HCl. The inset table shows binding energies for each energy minima and the Hirshfeld charge on each Au atom.
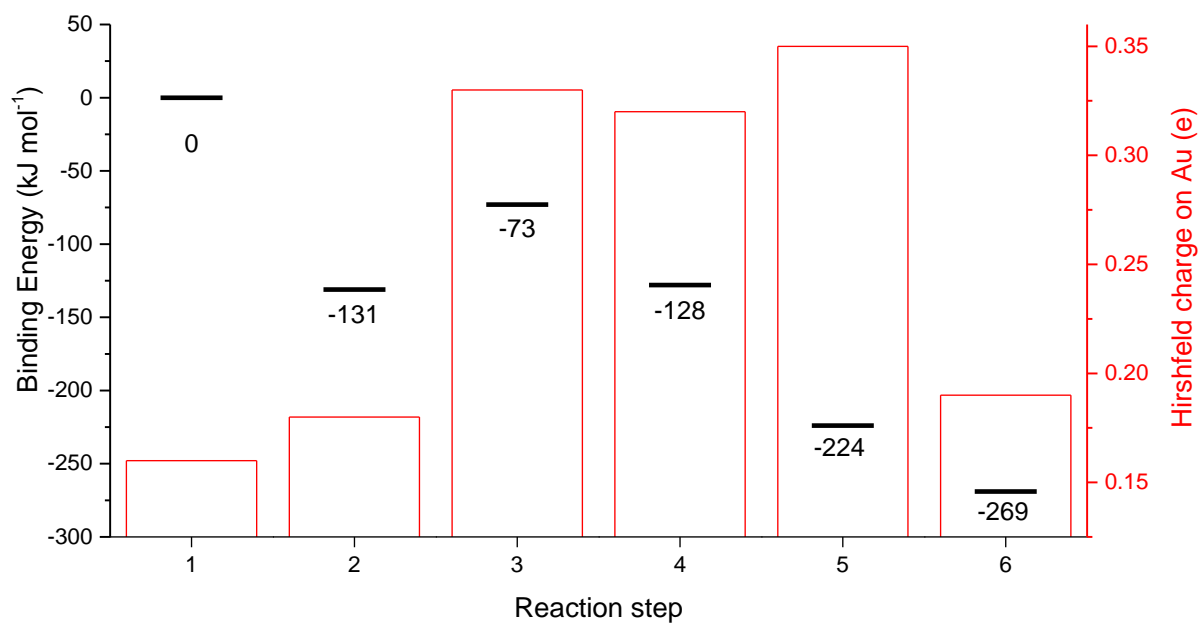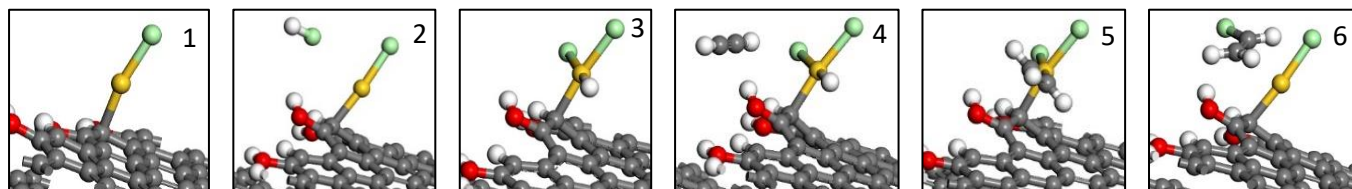
References

1.	P. Johnston, N. Carthey, G. J. Hutchings, *J. Am. Chem. Soc.* **137**, 14548-14557 (2015).
2.	R. Ciriminna, E. Falletta, C. Della Pina, J. H. Teles, M. Pagliaro,. *Angew. Chem. Int. Ed.* **55**,14210 –14217 (2016)
3.	G. J. Hutchings, *J. Catal.* **96**, 292-295 (1985).
4.	B. Nkosi, N. J. Coville, G. J. Hutchings, *Appl. Catal.* **43**, 33-39 (1988).
5.	http://www.mercuryconvention.org/.
6.	B. Nkosi *et al.*, *J. Catal.* **128**, 366-377 (1991).
7.	G. Hong *et al.*, *RSC Adv.* **6**, 3806-3814 (2016).
8.	M. Zhu *et al.*, *ACS Catal.* **5**, 5306-5316 (2015).
9.	X. Tian *et al.*, *RSC Adv.* **5**, 46366-46371 (2015).
10.	B. Nkosi, M. D. Adams, N. J. Coville, G. J. Hutchings, *J. Catal.* **128**, 378-386 (1991).
11.	X. Liu *et al.*, *Catal. Sci. Tech.* **6**, 5144-5153 (2016).
12.	S. Carrettin *et al., Adv. Synth. Catal.* **348**, 1283-1288 (2006)
13.	L. Huang *et al*., *Angwe. Chem, Int, Ed.* **55**, 4808-4813 (2016)
14.	A. S. K. Hashmi, *Gold Bulletin.* **36**, 3-9 (2003).
15.	M. Flytzani-Stephanopoulos, *Acc. Chem. Res.* **47**, 783-792 (2014).
16.	W. Deng, A. I. Frenkel, R. Si, M. Flytzani-Stephanopoulos, *J. Phys. Chem. C* **112**, 12834-12840 (2008).
17.	J. C. Fierro-Gonzalez, B. C. Gates, *J. Phys. Chem. B.* **108**, 16999-17002 (2004).
18.	J. Lu, C. Aydin, N. D. Browning, B. C. Gates, *Angew. Chem., Int. Ed.* **51**, 5842-5846 (2012).
19.	M. C. Blanco Jaimes, C. R. N. Böhling, J. M. Serrano-Becerra, A. S. K. Hashmi, *Angew. Chem., Int. Ed.* **52**, 7963-7966 (2013).
20.	M. C. Blanco Jaimes *et al.*, *Chem. Commun.* **50**, 4937-4940 (2014).
21.	A. S. K. Hashmi *et al.*, *Chem. - Eur. J.* **16**, 8012-8019 (2010).
22.	Supporting information is avaliable online (Experimental details, Tables S1-2, Figures S1 – 13, and references 32-44)
23.	S.-Y. Chang *et al.*, *RSC Adv.* **5**, 6912-6918 (2015).
24.	A. Pantelouris, G. Kueper, J. Hormes, C. Feldmann, M. Jansen, *J. Am. Chem. Soc.* **117**, 11749-11753 (1995).
25.	I. Berrodier *et al.*, *Geochim. Cosmochim. Acta* **68**, 3019-3042 (2004).
26.	O. Glemser, H. Sauer, Handbook of Preparative Inorganic Chemistry. *Academic Press* **2**, 1056 (1965).
27.	P. Hu, P. N. Duchesne, Y. Song, P. Zhang, S. Chen, *Langmuir* **31**, 522-528 (2015).
28.	N. Weiher *et al.*, *J. Am. Chem. Soc.* **129**, 2240-2241 (2007).
29.	M. Fernandez-Garcia, *Catal. Rev. - Sci. Eng.* **44**, 59-121 (2002).
30.	P. T. Bishop, N. A. Carthey, P. Johnston, WO 2013/008004A3, May 16, 2013.
31.	R. A. Bryce, J. M. Charnock, R. A. D. Pattrick, A. R. Lennie, *J. Phys. Chem. A.* **107**, 2516-2523 (2003).
32.	M. Conte *et al.*, *J. Catal.* **250**, 231-239 (2007).
33.	M. Pernpointner, A.S.K. Hashmi, *J. Chem. Theory Comput.* **5**, 2717–2725 (2009).
34.	A.S.K. Hashmi, *Angew. Chem. Int. Ed.* **51**, 12935 – 12936 (2012).
35.	A. Pantelouris, G. Kiiper, J Homes, C. Feldmann, M. Jansen, *J. Am. Chem. Soc.*, **117**, 11749-11753 (1995).

36.	D. Tibiletti, A. Amieiro-Fonseca, R. Burch, Y. Chen, J. M. Fisher, A. Goguet, C. Hardacre, P. Hu, D. Thompsett, *J. Phys. Chem. B,* **109**, 22553-22559 (2005)
37.	G.J. Sherborne, B.N. Nguyen, *Chemistry Central Journal* , **9**, 37 (2015)
38.	B. Ravel, M. Newville, *J. Synchrotron Radiat.*, **12**, 537−541 (2005)
39.	M. Newville, J. Synchrotron Radiat., **8**, 322−324 (2001).
40.	S. J. Clark, M. D. Segall, C. J. Pickard, P. J. Hasnip, M. J. Probert, K. Refson, M.C. Payne. *Zeitschrift fuer Kristallographie*, **220**, 567 (2005).
41.	N. Govind, M. Petersen, G. Fitzgerald, D. King-Smith, J. Andzelm, *Comput. Mater. Sci.*, **28**, 250 (2003).
42.	E.R. McNellis, J. Meyer, K. Reuter, *Phys. Rev. B*, **80**, 205414 (2009).
43.	A. Tkatchenko, M. Scheffler, *Phys. Rev. Lett.*, **102**, 073005 (2009).
44.	A.P. Seitsonen, A.M. Saitta, T. Wassmann, M. Lazzeri, F. Mauri, *Phys. Rev. B*, **82**, 115425 (2010).
45.	R. Burgess, C. Buono, P.R. Davis, R.J. Davis, T. Legge, A. Lai, R. Lewis, D.J. Morgan, N. Robinson, D.J. Willock, *J. Catal.*, **323**, 10 (2015).
46.	H. Kitagawa, N. Kojima, T. Nakajima, *J. Chem. Soc. Dalton Trans*., 3115 (1991)

47.	H. Kitagawa, N. Kojima, T. Nakajima, *J. Chem. Soc. Dalton Trans*., 3121 (1991)

Acknowledgments

Supplementary materials

Materials and Methods

Figs. SE1 and SE2

Figs. S1 to S13

Tables S1 and S2

References (35–47)